PERGAMON

Vision Research 39 (1999) 3444–3458

Vision Research

www.elsevier.com/locate/visres

Trichromatic opponent color classification☆

E.J. Chichilnisky [a,b,*], Brian A. Wandell [a]

[a] *Department of Psychology and Neuroscience Program, Stanford University, Stanford, CA 94305, USA*
[b] *The Salk Institute, 10010 North Torrey Pines Road, La Jolla, CA 92037, USA*

Received 4 March 1998; accepted 30 November 1998

Abstract

Stimuli varying in intensity and chromaticity, presented on numerous backgrounds, were classified into red/green, blue/yellow and white/black opponent color categories. These measurements revealed the shapes of the boundaries that separate opponent colors in three-dimensional color space. Opponent color classification boundaries were generally not planar, but their shapes could be summarized by a piecewise linear model in which increment and decrement color signals are combined with different weights at two stages to produce opponent color sensations. The effect of background light on classification was largely explained by separate gain changes in increment and decrement cone signals.

Keywords: Color; Opponent; Hue; Cancellation; Cone

1. Introduction

This paper describes quantitative measurements of how observers classify simple stimuli as red or green, blue or yellow, white or black. These mutually exclusive opponent colors, first described by Hering (Hering, 1878), are thought to reflect the representation of color in the central visual system. The goal of this work is to elucidate how the visual system combines signals from the three types of cone photoreceptors to create opponent color sensations.

This question was first addressed experimentally in the hue cancellation experiments of Jameson and Hurvich. They measured the amount of a standard stimulus that, combined with a test stimulus, caused the mixture to appear neither red nor green (similarly for blue/yellow; luminosity judgments were used for white/black). These measurements were interpreted using a linear model whose central assumption was that the magnitude of each opponent sensation is determined by a weighted sum of the quantum absorptions in each of the three cone types (Jameson & Hurvich, 1955). The linearity of opponent colors has been tested in a number of experiments, and significant failures have been observed (e.g. Larimer, Krantz & Cicerone, 1975; see Section 4). While the presence of a nonlinearity is certain, its form is not, so linear opponent models remain in use in spite of the empirical evidence. To clarify the rules governing opponent color classification, including important nonlinearities, the present work incorporates three main principles.

First, observers classified stimuli of moderate contrast presented on a variety of photopic backgrounds. This stimulus choice parallels the contrast variation in signals arriving at the eye in the natural world as well as in many applications. It differs from the conventional approach of fixing a single (usually dark) background and presenting stimuli of widely varying intensity. In a moderate contrast range one may observe a simpler but important aspect of visual system performance.

Second, a three dimensional description of stimuli was used to represent measurements and examine the workings of opponent mechanisms. This approach is more general than the approach used in early studies which were based on measurements with spectral lights. Representing stimuli in three-dimensional color space allows a compact and intuitive description of hue classifications: the classification boundary. The red–green classification boundary, for example, partitions the

☆ Data: ⟨http://white.stanford.edu/color/TOCC/⟩

* Corresponding author. Tel.: +1-619-4534100.
E-mail address: ej@salk.edu (E.J. Chichilnisky)

0042-6989/99/$ - see front matter
PII: S0042-6989(99)00033-4

three-dimensional space of visible colors into two regions corresponding to red and green sensations (similarly, blue/yellow and white/black). This geometric representation provides a complete description of opponent color classification (Knoblauch, Sirovich & Wooten, 1985).

Third, a geometric description of classification boundaries was developed. This can be used to test models of the neural computations that underlie opponent color sensations. Also, because light adaptation influences color appearance it changes the shape of classification boundaries. A geometric description of these changes can be used to test models of adaptation.

2. Methods

2.1. Observers and stimuli

Two paid male undergraduates (ES and RR) and one paid female of similar age (KS) participated in the experiment over a period of several months. These observers had normal color vision according to the Ishihara plates (Ishihara, 1977). Observers RR and KS used their normal untinted corrective eyewear during experiments.

Observers viewed a cathode ray tube (CRT) computer monitor from a distance of 23 cm in a dark room. The uniform background on the display occupied the central 59 horizontal and 45 vertical degrees of visual angle. Square test stimuli 2.5° on a side were flashed at the center of this background for 375 ms. The remainder of the visual field was occupied by a hood lined with wrinkled aluminum foil (75% spectrally flat reflectance) which acted as a partial diffuser. Because the test stimulus covered only 0.2% of the area of the display and was only present for brief periods, the light reflected from the hood had approximately the same relative spectral power distribution as did the background on the display. Backgrounds were chosen to span the range available on the display while allowing test stimuli of many different colors to be presented. The average background luminance used was about 50 cd/m^2. The color names of backgrounds reported in the text describe their appearance to the authors when viewed at a distance in a dark room. Observers signalled responses using a hand held button box.

2.2. Task and experimental design

For the red–green task observers were instructed to classify flashed targets as either reddish or greenish. Observers found the task fairly easy and did not indicate a desire to classify stimuli as both reddish and greenish. Similarly for the blue–yellow task. For the white–black task, observers were asked to indicate whether the flashed target contained a component of white or black. Observers had more difficulty with this task and found it helpful to compare the lightness of the target to that of the background. Classification data were used only after each subject reported clear and unchanging criteria. After a few sessions, naive observers ES and KS as well as the authors made stable white–black classifications. Experienced observer RR found the white–black task difficult and did not perform it.

A session consisted of 48 trials in which only one type of classification was performed; here we use red–green classification as an example. Sessions were performed in contiguous blocks of four, in which the background light was fixed. Observers began a block by viewing the background for 2 min, after which it generally took on a desaturated appearance. The observer then began a session by viewing a stimulus $\vec{A}$ chosen by the experimenter to be plainly reddish, and a second stimulus $\vec{B}$ chosen to be plainly greenish. The observer confirmed this description of $\vec{A}$ and $\vec{B}$, or aborted the session. All stimuli in the remainder of the session were created by mixtures of these two primaries, e.g. $\alpha\vec{A} + (1-\alpha)\vec{B}$ where $0 \leq \alpha \leq 1$ is the *mixture fraction*. When represented in a three-dimensional color space, each stimulus fell on a line between $\vec{A}$ and $\vec{B}$.

The observer then coarsely adjusted the mixture fraction α to a value where the stimulus appeared roughly in *equilibrium*, i.e. neither reddish nor greenish. A randomized value near this value of α was used as a starting point for subsequent trials. In each trial the observer classified a flashed stimulus $\alpha\vec{A} + (1-\alpha)\vec{B}$ as reddish or greenish. The observer could take as long as desired for each classification; typically each trial lasted several seconds. The next trial was initiated immediately after the response. During trials, the mixture fraction α was adjusted over about seven levels according to the observer's classifications using a double-random staircase procedure which kept the stimulus near equilibrium.

The data from each session were used to obtain one estimated equilibrium stimulus (see below). For each observer and each background and each task (red–green, blue–yellow, white–black) about 24 equilibria were obtained, each using different primaries. Pairs of primaries were chosen to span the range available on the display. For example, in the red–green task one choice of primaries might appear purple and aquamarine, another might appear orange and green. Each observer repeated measurements once or twice for each set of primaries on a specific grey background to obtain an estimate of measurement variability. From observer ES (KS, RR), a total of 480 (390, 568) red–green, 501 (404, 583) blue–yellow, and 514 (352, 0) white–black equilibria were obtained on a total of 19 (13, 19) backgrounds.

2.3. Estimating opponent color equilibria and variability

During each session, as α increased from 0 to 1 the probability $P(\alpha)$ that the observer responded red increased from 0 to 1. The value of the mixture fraction that would in principle have yielded exact red–green equilibrium was estimated as follows. First, a maximum likelihood method was used to estimate the mean and standard deviation parameters of a cumulative Gaussian fit to $P(\alpha)$ (Watson, 1979). The value $\bar{\alpha}$ for which $P(\bar{\alpha}) = 0.5$ was obtained from this fit. The stimulus given by $\bar{\alpha}\vec{A} + (1-\bar{\alpha})\vec{B}$ was taken to be an equilibrium stimulus.

When fitting models each measurement $\bar{\alpha}$ was weighted by an estimate of its reliability (see below) because the variance of equilibrium measurements depended on the primaries used as well as on the background light. For example, red–green judgments of nearly achromatic stimuli were less variable than red–green judgments of bluish stimuli. The large number of different stimulus conditions precluded obtaining direct estimates of the variability of $\bar{\alpha}$ for each condition. Since psychometric functions with shallower slopes should give rise to more variable estimates of the midpoint, it was assumed that the standard deviation $\hat{\sigma}$ of the estimated equilibrium mixture fraction $\bar{\alpha}$ was proportional to the standard deviation parameter of the cumulative Gaussian fit to the psychometric function $P(\alpha)$ (see above). Since only the relative values of $\hat{\sigma}$ under different conditions were relevant for hypothesis testing, the constant of proportionality was taken to be one.

However, this estimate of $\hat{\sigma}$ was plainly too small in sessions where the values of α used were widely separated. For example, in some cases, for all measured values of $\alpha > \bar{\alpha}$ the observer gave only red responses, and for all values $\alpha < \bar{\alpha}$ the observer gave only green responses. The cumulative Gaussian function that best fits such data has a standard deviation parameter of zero. Since $\hat{\sigma} = 0$ seemed unrealistic and made model fits unstable, $\hat{\sigma}$ was not permitted to be smaller than the largest standard deviation parameter of the cumulative Gaussian fit to $P(\alpha)$ that could have generated the observations with probability 0.05, assuming that each trial was an independent binomial draw with mean value $P(\alpha)$. This minimum value for $\hat{\sigma}$ depends on the number of trials, the spacing of the values of α used, and the observed classifications.

2.4. Data representation

The spectral composition of a stimulus is represented by either the monitor phosphor intensities ($R\ G\ B$) used to create the stimulus (*monitor coordinates*), or values proportional to the quantum absorptions ($L\ M\ S$) induced by the stimulus in each of the three types of cone photoreceptors (*cone coordinates*). The light transiently added to or subtracted from the background to create the test stimulus is also represented by three numbers, e.g. ($\Delta R\ \Delta G\ \Delta B$) or ($\Delta L\ \Delta M\ \Delta S$).

The monitor coordinates and the cone coordinates of stimuli are related by a 3×3 linear transformation whose entries are proportional to the quantum absorptions induced by each monitor phosphor in each of the three cone types (Wandell, 1995). This was calculated

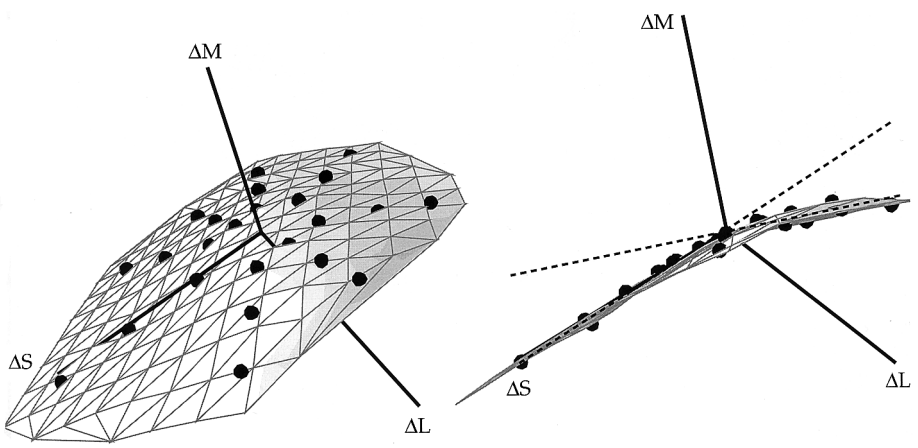

Fig. 1. Red–green classification boundary. The three-dimensional coordinates of each point represent the cone quantum absorptions associated with a red–green equilibrium stimulus, expressed as differences ($\Delta L\ \Delta M\ \Delta S$) from the background quantum absorptions. A smooth surface passing through the points is shown to aid visualization (see Section 2). The two panels show rotated views of the same data and surface. Additional dashed lines in the right view are drawn to emphasize the bend in the data. Error bars extending from points indicate ± 1 standard deviation of the psychometric function associated with the equilibrium measurement, and point in a direction joining the two stimulus primaries used (see Section 2). In this figure most error bars are smaller than the points. A total of 24 equilibrium measurements are shown though some are obscured by the surface. The background had a greenish appearance when viewed from a distance in a dark room. Background cone coordinates: (0.103 0.103 0.0617). Axis lengths: (0.0323 0.0327 0.0459). Observer: ES.

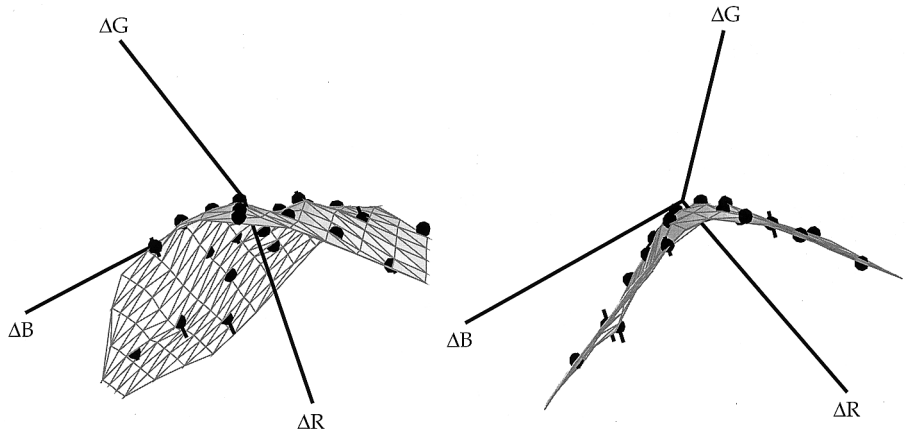

Fig. 2. Red–green classification boundary. Same data as Fig. 1, in monitor coordinates; the three-dimensional coordinates of each point represent the red, green and blue monitor phosphor intensities of a red–green equilibrium stimulus, expressed as differences ($\Delta R\ \Delta G\ \Delta B$) from background phosphor intensities. Background gun intensities relative to maximum: (0.2 0.85 0.5). Axis length: 0.51. Observer: ES.

by multiplying and integrating measurements of each phosphor emission spectrum (in watts/sr/nm, measured between 370 and 730 nm at 1 nm resolution) by the spectral sensitivity of each cone type (Stockman, MacLeod & Johnson, 1993) normalized to a maximum of 1, yielding:

$$\begin{pmatrix} L \\ M \\ S \end{pmatrix} = \begin{pmatrix} 0.044490 & 0.098416 & 0.020081 \\ 0.017180 & 0.099258 & 0.029193 \\ 0.001817 & 0.007694 & 0.111120 \end{pmatrix} \begin{pmatrix} R \\ G \\ B \end{pmatrix}$$

where ($R\ G\ B$) coordinates between 0 and 1 represent the gamut of the display and ($L\ M\ S$) quantum absorptions are in arbitrary units.

The shaded surfaces shown near the data in figures were created as follows. The best-fitting plane to each three-dimensional data set was obtained. Raw data vectors ($a\ b\ c$) were linearly transformed to a new representation, $(p\ q\ r) = (a\ b\ c)\ M$, in which the first two coordinates ($p\ q$) are projections onto two orthogonal basis vectors within the plane. The ($p\ q\ r$) values were then interpolated using triangle-based cubic interpolation to create a set of points ($p'\ q'\ r'$) whose ($p'\ q'$) values constitute a finely spaced grid in the plane. A Delaunay triangularization was created from the interpolated points ($p'\ q'\ r'$) combined with the original data ($p\ q\ r$). The vertices of these triangles were then converted back to the original coordinate frame using the inverse of M. To create triangles extending beyond the data, extreme data points were first replicated with a scaling of 1.4 (replicated points are not shown in the figures). For the pooled data of Figs. 10 and 11 triangles were created from model predictions rather than data. The resulting collection of triangles, with data superimposed, was imaged using *Geomview* software produced by the Geometry Center at the University of Minnesota.

2.5. Equipment and calibration

Stimuli were displayed on a Hitachi HM-4320-D color computer monitor controlled by an eight-bit Number Nine Graphic Systems video card refreshed at 88 Hz (non-interlaced) at a spatial resolution of 640 (horizontal) × 480 (vertical) pixels. The luminance of the display with all guns set to maximum intensity was 104 cd/m^2. Intensity stability was checked every few days using a Minolta ChromaMeter.

The spectral emission of the monitor phosphors was measured using a PhotoResearch PR-703A Spectral Scanner, and the digital control value to phosphor intensity relation (gamma curve) using a PhotoResearch 2009 Tele-Photometer. The CRT calibration procedure used is described by Brainard (Brainard, 1989; see also Wandell, 1995). Between calibrations gamma curves and gun spectra typically changed no more than a few percent.

As with many CRT monitors, the Hitachi display intensity was not spatially uniform, but peaked in the center and decreased smoothly to about 80% of maximum at the edges of the display. Calibration measurements were made at the center of the screen where test stimuli were presented. No attempt was made to correct for the spatial intensity inhomogeneity.

2.6. Model fitting

The models that will be considered for hue classification all make predictions for the mixture fraction required to bring the mixture of a pair of primary stimuli $\vec{A}$ and $\vec{B}$ into equilibrium. That is, any given model predicts a value $\hat{\alpha}$ which will cause the mixture $\hat{\alpha}\vec{A} + (1-\hat{\alpha})\vec{B}$ to be classified red or green with equal probability. To obtain model fits to the data that are independent of the color coordinate frame in which stimuli are represented, and which take into account

the reliability of each measurement, model parameters were chosen to minimize the difference between the measured mixture fraction $\bar{\alpha}$ and the model prediction $\hat{\alpha}$, expressed in units of the estimated standard deviation $\hat{\sigma}$ of $\bar{\alpha}$: $e = (\hat{\alpha} - \bar{\alpha})/\hat{\sigma}$. This distance will be referred to as the *psychometric distance* between model prediction and data, or as the *psychometric error* associated with the model prediction. Assuming $\hat{\sigma}$ is an accurate estimate of the standard deviation of the measurement $\bar{\alpha}$, e will be approximately normally distributed with unit variance, and the sum squared error (SSE) value

$$\sum_{i=1}^{n} (e_i)^2$$

summed over n equilibrium measurements will be approximately χ^2 distributed with n degrees of freedom. Model parameters were chosen to minimize the SSE, since this provides a maximum likelihood estimate. This procedure is equivalent to minimizing the root mean square (RMS) psychometric error:

$$\sqrt{\frac{1}{n}\sum_{i=1}^{n} (e_i)^2}$$

The RMS error rather than the SSE is used to report the quality of the model fits because (a) it has the same units as individual psychometric errors; and (b) it does not depend on the total number of measurements.

Though these statistical calculations were used to assess the quality of models, rigorous statistical hypothesis testing was not applied to models because the requisite distribution assumptions are very unlikely to hold.

Fitting models to equilibrium data involved iterative searches for parameters that minimized the RMS psychometric distance between model predictions and data. Because the searches sometimes encountered local minima, it is not certain that these were the best possible fits of the model. Fits were obtained using two optimization algorithms and a number of randomized initial parameters.

3. Results

3.1. Opponent color classification boundaries

Opponent color classification boundaries were generally nonplanar surfaces that passed near or through the background and varied with background light. The shape of one red–green classification boundary measured on a greenish background is shown in Fig. 1. The equilibrium stimuli shown appeared bluish, yellowish, and various shades of grey. The left view shows the data dispersed on a two-dimensional surface. The right view shows that the data collapse onto a bent line when viewed from a particular angle. Thus in three dimensions these data fall near a bent plane. Since all stimuli visible to the observer may be represented in this three-dimensional color space, the boundary formed by the data summarizes the red–green classification behavior of this observer in these experimental conditions.

The primary bend in the red–green classification boundary of Fig. 1 occurs near the *achromatic locus*, i.e. the set of stimuli which appear neither red, green, yellow, nor blue. This locus consists of points near the

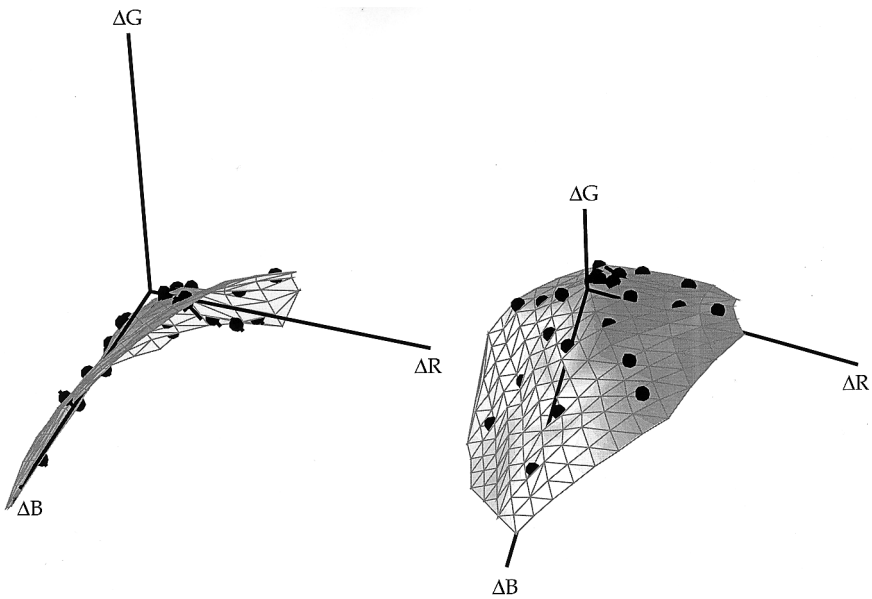

Fig. 3. Red–green equilibrium stimuli viewed on a yellowish green background. Background gun intensities relative to maximum: (0.44 0.69 0.22). Number of points: 24. Axis length: 0.71. Observer: RR. Other details as in Fig. 2.

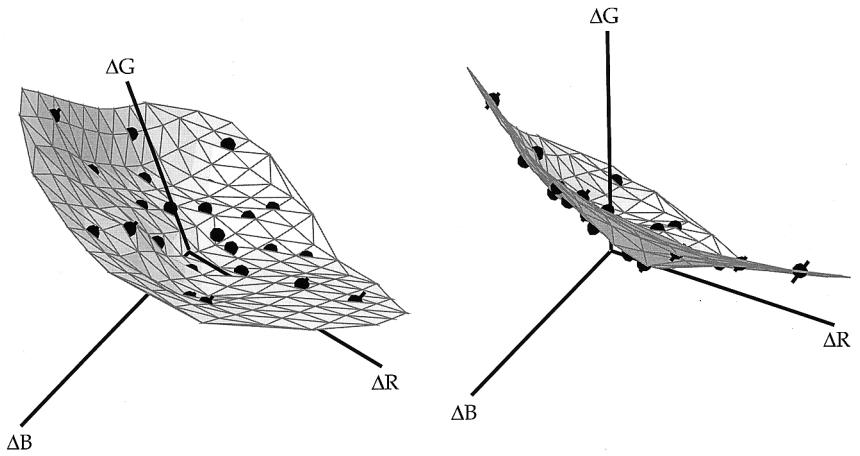

Fig. 4. Blue–yellow equilibrium stimuli viewed on a purple background. Background gun intensities relative to maximum: (0.47 0.23 0.72). Number of points: 24. Axis length: 0.49. Observer: RR. Other details as in Fig. 2.

line defined by $\Delta L = \Delta M = \Delta S$. It is oriented approximately orthogonal to the printed page in the right panel of Fig. 1, emanating from the origin. The data to the left of the bend (bluish stimuli) and to the right of the bend (yellowish stimuli) each appear to fall on a roughly planar surface (Burns, Elsner, Pokorny & Smith, 1984; Mausfeld & Niederee, 1993).

3.2. Opponent classification is generally not linear

If the visual system computed opponent colors linearly, the classification boundary in Fig. 1 would be a plane. Suppose the red–green signal RG was a linear combination of cone quantum absorptions, plus an optional constant:

$$RG = aL + bM + cS + d \quad (1)$$

Then points falling on the red–green boundary (i.e. zero red–green sensation) would satisfy $RG = 0$. This is the equation of a plane in $(L\ M\ S)$ space. The non-planarity of the boundary in Fig. 1 is inconsistent with a linear opponent color computation.

This deviation from planarity was visually significant. Were opponent classifications linear, the mixture of two equilibrium stimuli would also be in equilibrium. The mixture of two extreme points on the surface in Fig. 1 predicted an intermediate equilibrium stimulus which was more than 12 psychometric function standard deviations away from the measured equilibrium (see Section 2). In other words, this mixture would easily be classified red by the observer on all trials.

The non-planarity of these data confirms previous studies showing that red–green opponent color classification is not generally based on a linear combination of cone absorptions (e.g. Ayama, Kaiser & Nakatsue, 1985; see Section 4). It also indicates that opponent classification is not generally based on a linear combination of differences between cone signals and a neutral point (Walraven, 1976), since Eq. (1) includes this case.

3.3. Shapes of classification boundaries

Additional features of classification boundaries are most easily visualized by examining the monitor coordinates $(R\ G\ B)$ of equilibrium stimuli. Though $(L\ M\ S)$ coordinates are more physiologically interpretable, $(R\ G\ B)$ coordinates are more evenly dispersed in plots, and equidistant points more closely approximate equally distinguishable stimuli. Since $(R\ G\ B)$ and $(L\ M\ S)$ coordinates are related by a linear transformation (see Section 2), the qualitative features of boundaries discussed here do not depend on the coordinate frame in which data are represented. For example, Fig. 2 shows the data from Fig. 1 in $(R\ G\ B)$ coordinates. The non-planarity of these data relative to measurement error is equally statistically significant in both representations, since measurement error was estimated in units that do not depend on the coordinate frame (see Section 2). But the bend is more obvious in Fig. 2. More subtle features of classification boundaries are substantially easier to see in $(R\ G\ B)$ coordinates, so all remaining equilibria are plotted this way.

Classification boundaries often had more than a single bend. An example is the red–green boundary shown in Fig. 3. The surface has a significant bend along the achromatic locus but is not simply a bent plane. In three dimensions this boundary appears roughly conical, with its concave side oriented down in the right panel. Similar shapes can be seen in the blue–yellow boundary of Fig. 4 and the white–black boundary of Fig. 5, with concave sides pointing up in the right panel of these figures.

Large systematic deviations from planarity were observed in the red–green and blue–yellow boundaries of observer ES (19 backgrounds), and red–green boundaries of observer RR (13 backgrounds). Smaller but systematic deviations were observed in the blue–yellow boundaries of observer RR and white–black

boundaries of observer ES. For these observers the concave side of red–green boundaries always corresponded to stimuli classified as red (e.g. the lower right side of the right panels in Figs. 2 and 3). That is, the mixture of two red–green equilibrium stimuli could result in a reddish stimulus, but not a greenish stimulus (Burns et al., 1984). This conclusion was supported by fitting each classification boundary with an elliptical cone (conical surface with elliptical orthogonal cross-sections) and examining the orientation of the best fit (not shown). This analysis also revealed that the concave side of blue–yellow boundaries for these observers corresponded to stimuli classified as yellow (e.g. Fig. 4) (Burns et al., 1984; DeValois, DeValois, Switkes & Mahon, 1997). For observer ES, the concave side of white–black boundaries tended to correspond to stimuli classified as white (e.g. Fig. 5).

However, some classification boundaries were nearly planar. An example is the white–black boundary shown in Fig. 6. The left view shows equilibrium stimuli dispersed on a two-dimensional surface. The right view shows that the data collapse onto a line when viewed from a particular angle, indicating a planar surface. An example of a roughly planar blue–yellow boundary is shown in Fig. 7. Classification boundaries from observer KS were generally not distinguishable from planes. This conclusion was supported by the observation that elliptical cones fitted to this observer's classification boundaries were not systematically oriented in one direction, and provided only a slightly better fit than planes (not shown). This indicates a qualitative difference in the opponent colors classifications of different observers.

3.4. Classification boundaries do not always contain the background

Most classification boundaries such as the one in Fig. 2 passed through or very near the origin, which represents the background. Because the background for the data in Fig. 2 was not in equilibrium (it appeared greenish), one interpretation of this observation is that hue classifications were based on the difference between the test stimulus and background light. Walraven refers to this as discounting the background (Walraven, 1976). However, some boundaries did not pass through the origin. An example is the blue–yellow boundary shown in Fig. 8. The left view shows the data dispersed on a two-dimensional surface. The right view shows that the surface containing the data does not include the origin. Thus opponent classifications are not based exclusively on the difference between test stimulus and background light (Shevell, 1978, 1980).

3.5. Classification boundaries vary with background light

As expected, the shapes of classification boundaries are affected by background light. Fig. 9 shows how the red–green classification boundary for one observer changed when stimuli were viewed on a pink background or a green background.

3.6. Modeling the shapes of classification boundaries

The shapes of classification boundaries depend on the opponent computations performed by the visual system. Therefore, models of boundary shapes may

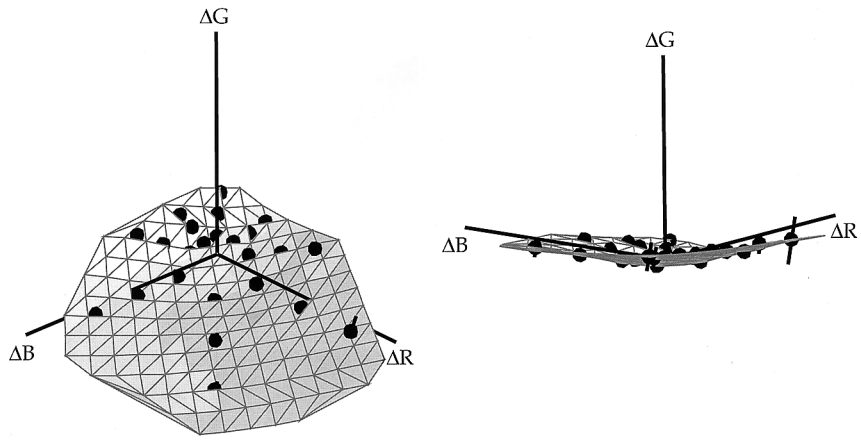

Fig. 5. White–black equilibrium stimuli viewed on a grey background. Background gun intensities relative to maximum: (0.27 0.24 0.32). Number of points: 24. Axis length: 0.63. Observer: ES. Other details as in Fig. 2.

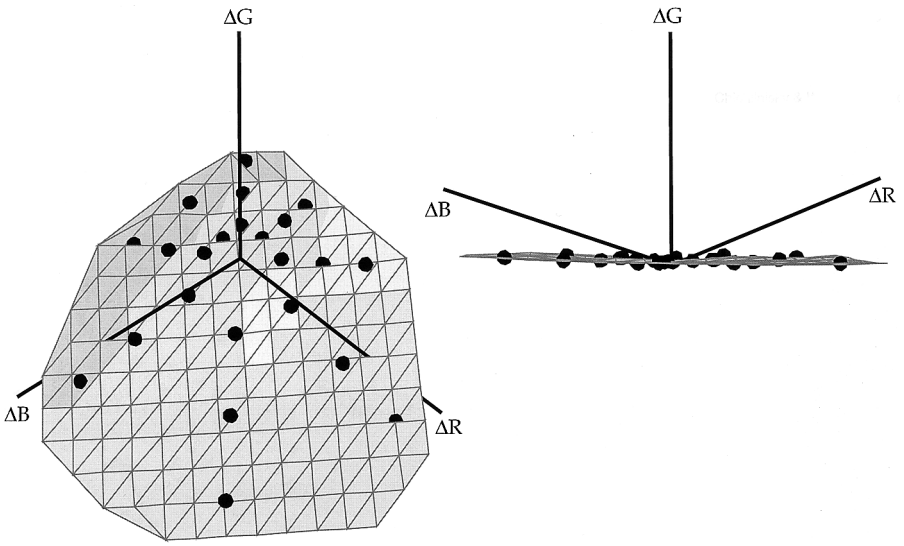

Fig. 6. White–black equilibrium stimuli viewed on a grey background. Background gun intensities relative to maximum: (0.27 0.24 0.32). Number of points: 24. Axis length: 0.59. Observer: KS. Other details as in Fig. 2.

help elucidate these computations. Boundary shapes were reasonably well described using the following piecewise linear model for hue classification.

3.7. Model specification

The model transforms a stimulus into a hue classification. Each stimulus is represented by the quantum absorptions ($L\ M\ S$) it induces in each of the three types of cone photoreceptor. The first stage of the model computes the difference between ($L\ M\ S$) and a neutral point, ($\bar{L}\ \bar{M}\ \bar{S}$).

$$(\dot{L}\ \dot{M}\ \dot{S}) = (L\ M\ S) - (\bar{L}\ \bar{M}\ \bar{S}) \tag{2}$$

A common neutral point is postulated for red–green, blue–yellow and white–black classifications on each background. (For these experiments, the neutral point is not very different from the background cone absorptions (Walraven, 1976; Shevell, 1978)). The signals ($\dot{L}\ \dot{M}\ \dot{S}$) are segregated into increment (positive) and decrement (negative) components, multiplied by separate gain factors (Mausfeld & Niederee, 1993; Chichilnisky & Wandell, 1996), and recombined to create intermediate signals:

$$\begin{array}{rll} L^* = g_L^{\oplus}\dot{L} & \text{for} & \dot{L} > 0 \\ \quad g_L^{\ominus}\dot{L} & \text{for} & \dot{L} \le 0 \\ M^* = g_M^{\oplus}\dot{M} & \text{for} & \dot{M} > 0 \\ \quad g_M^{\ominus}\dot{M} & \text{for} & \dot{M} \le 0 \\ S^* = g_S^{\oplus}\dot{S} & \text{for} & \dot{S} > 0 \\ \quad g_S^{\ominus}\dot{S} & \text{for} & \dot{S} \le 0 \end{array} \tag{3}$$

Gain values (e.g. $g_L^{\oplus}$, and $g_L^{\ominus}$) are non-negative and depend on the background light. The model classifies a stimulus as reddish if the intermediate signals satisfy two inequalities:

$$\begin{aligned} a_0 L^* + b_0 M^* + c_0 S^* &> 0 \\ a_1 L^* + b_1 M^* + c_1 S^* &> 0 \end{aligned} \tag{4}$$

for some constants a_0, b_0, c_0, a_1, b_1, c_1. Otherwise, the model classifies the stimulus as greenish. Similar inequalities are postulated for blue–yellow and white–black classifications. This model of hue classification will be referred to as the increment–decrement opponency or IDO model.

3.8. Model boundary shape

Consider the classification boundary that separates stimuli classified by the IDO model as reddish from stimuli classified as greenish. If stimuli are plotted in a space whose axes are the intermediate signals ($L^*\ M^*\ S^*$), then because the opponent computation of Eq. (4) consists of two linear inequalities, the boundary separating reddish from greenish stimuli takes the form of a bent plane: one planar portion of this surface arises from the first inequality, the other portion from the second. When plotted in a space whose axes are the raw cone coordinates ($L\ M\ S$) (or a linear transformation of them, such as ($R\ G\ B$)), the classification boundary contains three additional bends at the transition from increments (e.g. $\dot{L} > 0$) to decrements (e.g. $\dot{L} < 0$), introduced by the asymmetric gain on increments (e.g. $g_L^{\oplus}$) and decrements (e.g. $g_L^{\ominus}$). The angle of each bend depends on the magnitude of this asymmetry. Therefore the IDO model predicts a piecewise planar classification boundary formed by a plane

bent four times, with each bend passing through the neutral point.Model evaluation

The piecewise planar surface predicted by the IDO model provided a good approximation to the observed shapes of classification boundaries. This finding was quantified by selecting model parameters to minimize the root mean square (RMS) psychometric distance between model predictions and measured classification boundaries (see Section 2). Data from each observer and each background were fitted separately, with common neutral points and increment/decrement gain enforced for all three types of hue classification on each background. Pooled RMS differences between model predictions and measurements are shown in Table 1. For observers KS and ES, 18 parameters determined all three model boundaries (red–green, blue–yellow, and white–black) on each background, whereas these observers usually made 72 total equilibrium settings on each background. For RR, 14 parameters determined two model boundaries (red–green and blue–yellow) on each background, whereas RR usually made 48 equilibrium measurements per background.

To evaluate the quality of the model fits relative to measurement error, the variability of repeated measurements is also given in Table 1. These were obtained with one to three repeats of each equilibrium measurement on a neutral grey background. The variability in repeated measurements was similar to the errors associated with the IDO model predictions. In fact, most of the IDO model errors were smaller. Two factors may contribute to this. First, repeat measurements were made across multiple days, while most model fits were made to classifications performed within one or two days. Hue classifications may have larger day-to-day than within-day variability. Second, the large number of model parameters compared to the number of measurements for each boundary may result in over-fitting. Thus these data should not be taken as strong empirical support for the IDO model, but as a demonstration of the adequacy of a piecewise planar surface for describing the shapes of classification boundaries.

3.9. Modeling the effect of background light

The dependence of opponent classification boundary shapes on background light could arise from changes in the neutral point and the gain of cone signals due to light adaptation (e.g. Werner & Walraven, 1982). Were this true, classification boundaries measured on different backgrounds should merge into a single boundary when the coordinates of equilibrium stimuli are corrected for the effects of background light. To test this hypothesis required an assumption about the functional form of these effects.

3.10. Model specification

Previous experiments in similar conditions (Chichilnisky, 1995; Chichilnisky & Wandell, 1996) suggested that increment and decrement cone signal gain may vary differently with background light, each according to a generalized Weber–Fechner (GWF) relation (Fechner, 1860). Accordingly, the gain of increment and decrement $\dot{L}$ signals was assumed to vary with the background cone absorptions ($L_B\, M_B\, S_B$) as follows:

$$g_L^{\oplus} = \frac{\rho^{\oplus}}{\sigma^{\oplus} + \lfloor \alpha^{\oplus} L_B + \beta^{\oplus} M_B + \gamma^{\oplus} S_B \rfloor}$$

$$g_L^{\ominus} = \frac{\rho^{\ominus}}{\sigma^{\ominus} + \lfloor \alpha^{\ominus} L_B + \beta^{\ominus} M_B + \gamma^{\ominus} S_B \rfloor} \quad (5)$$

Here, the notation $\lfloor x \rfloor$ denotes half-rectification: $\lfloor x \rfloor = x$ if $x > 0$, and $\lfloor x \rfloor = 0$ otherwise. The coefficient $\beta^{\oplus}$, for example, indicates how strongly M cone background absorptions reduce $\dot{L}$ increment signal gain relative to gain in darkness, which is $\rho^{\oplus}/\sigma^{\oplus}$. Similar relations were postulated for the gain of increment and decrement $\dot{M}$ and $\dot{S}$ values. These gain values

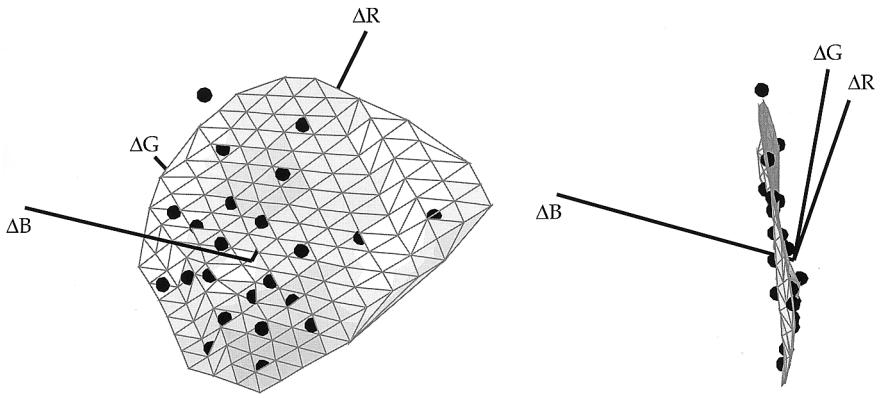

Fig. 7. Blue–yellow equilibrium stimuli viewed on a yellowish green background. Background gun intensities relative to maximum: (0.44 0.69 0.22). Number of points: 24. Axis length: 0.65. Observer: KS. Other details as in Fig. 2.

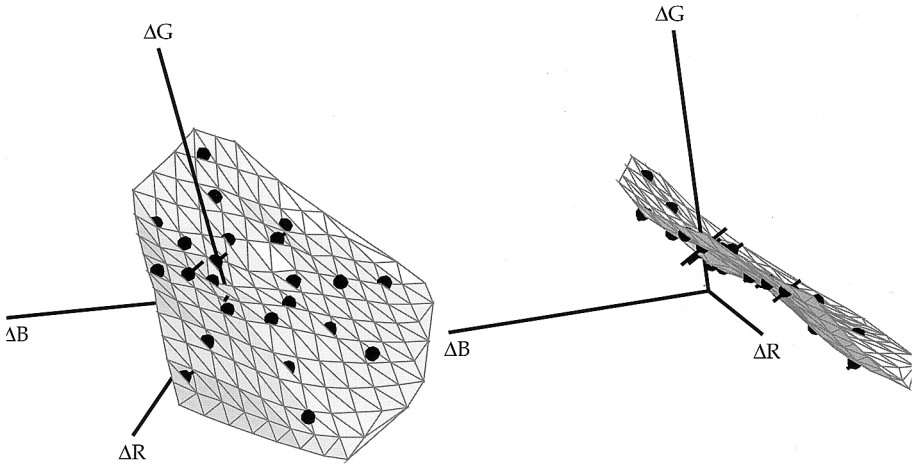

Fig. 8. Blue–yellow equilibrium stimuli viewed on a bluish background. Background gun intensities relative to maximum: (0.39 0.41 0.82). Number of points: 24. Axis length: 0.56. Observer: RR. Other details as in Fig. 2.

were assumed to be common for all three classification tasks (red–green, blue–yellow, white–black) on each background. The neutral point was assumed to be a fixed offset from the background, this offset was the same for all backgrounds.

3.11. Model evaluation

This adaptation model was evaluated by expressing data from each background as differences from the best-fit model neutral point (Eq. (2)) and correcting them for best-fit model gain values (Eqs. (3) and (5)), pooling the corrected data, and fitting the IDO model (Eq. (4)) to the surface formed by the pooled data. Common gain values and neutral point were enforced for red–green, blue–yellow and white–black data from each observer. In all, 36 independent parameters were required to fit red–green, blue–yellow and white–black equilibria from all backgrounds for observers ES and KS (1495 and 1146 measurements, respectively); 32 independent parameters were required to fit red–green and blue–yellow equilibria on all backgrounds for observer RR (1151 equilibrium measurements). The pooled, corrected red–green equilibria from one observer are shown in Fig. 10. Neutral point and GWF gain corrections cause these data to fall near a common bent surface. The classification boundary predicted by the IDO model is shown in the figure. This provides a reasonable fit, though systematic deviations can be observed at the extremes. Pooled, corrected white–black data from another observer are shown in Fig. 11. In this case, the IDO model boundary shown in the figure is nearly planar (a plane is a special case of the piecewise planar model boundary) and fits the data well.

The errors associated with the combined IDO/GWF model fits to data from each subject on all backgrounds are shown in Table 1. These are similar to the variability in repeated measurements shown in the table. For comparison, the table also shows the errors associated with a null model: pooling cone coordinates of equilibrium stimuli expressed as differences from a single background-independent neutral point, and fitting the IDO model to the pooled data. The errors associated with this null model are much higher than those associated with the combined IDO/GWF model, indicating that the latter model captures trends in the data.

Simply expressing equilibrium measurements as offsets from background-dependent neutral points brought the data from different backgrounds coarsely into register (not shown). Additionally correcting for GWF gain values helped correct for changes in boundary shape such as that shown in Fig. 9. These findings are consistent with the idea that the effect of background light on the neutral point and on increment and decrement cone signal gain can largely explain how classification boundaries change with background light.

4. Discussion

4.1. Approximate homogeneity, failure of superposition

The results reported here extend the evidence for nonlinearities in opponent color classification and describe them more fully across many background conditions. Many studies have demonstrated that opponent color classifications of intense, saturated lights do not satisfy the key predictions of a linear model: homogeneity and superposition. The homogeneity prediction is that an equilibrium stimulus should remain in equilibrium when its intensity is varied. Certain stimuli do satisfy homogeneity: achromatic stimuli (neither red nor green, blue nor yellow) remain in equilibrium over a large intensity range (Walraven & Werner, 1991) as do certain unique yellows (neither red nor green)

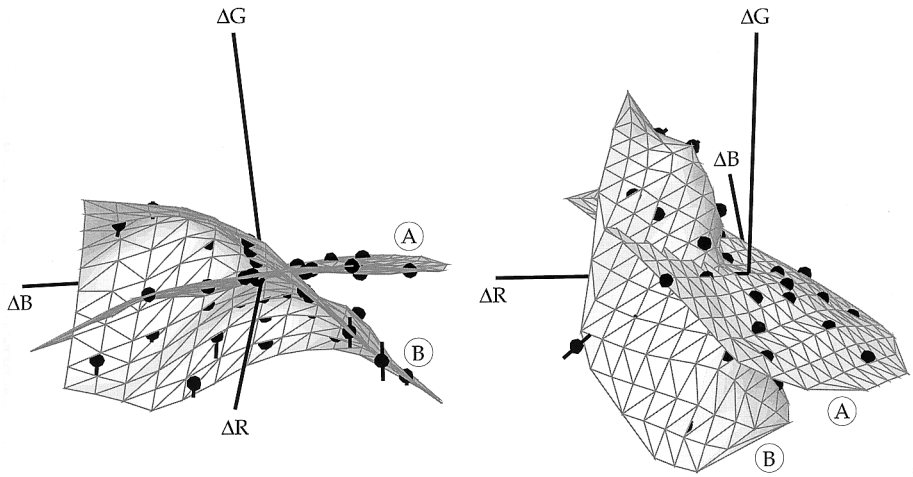

Fig. 9. Red–green classification boundaries measured on two different backgrounds. Points on boundary marked A (B) represent red–green equilibrium stimuli viewed on a pink (green) background. The coordinates of each point represent the monitor phosphor intensities comprising the stimulus, expressed as differences from their respective background gun intensities. Background gun intensities relative to maximum: A (0.82 0.29 0.54); B (0.2 0.74 0.53). Number of points: A, 21; B, 24. Axis length: 0.55. Observer: ES. Other details as in Fig. 2.

(Larimer, Krantz & Cicerone, 1974; Cicerone, Krantz & Larimer, 1975; Ejima & Takahashi, 1985). However some red–green and blue–yellow equilibria do not satisfy homogeneity (Cicerone et al., 1975; Larimer et al., 1975; Ejima & Takahashi, 1985). The superposition prediction of the linear model is that the sum of two distinct equilibrium stimuli should also be in equilibrium. This hypothesis has been rejected repeatedly in both dark-adapted and photopic conditions (Werner & Wooten, 1979; Ikeda & Ayama, 1980; Burns et al., 1984; Ayama et al., 1985; Ayama & Ikeda, 1986). More recent evidence has also demonstrated increment–decrement asymmetries in red–green cancellation (Mausfeld & Niederee, 1993) and achromatic settings (Chichilnisky & Wandell, 1996), inconsistent with linearity. Therefore opponent color computations on intense saturated lights cannot be understood with a linear model.

However, many previous equilibrium measurements were made using zero intensity backgrounds or incremental test stimuli that exceeded the background intensity by several orders of magnitude. The non-planar shapes of classification boundaries described here show that linear models cannot explain opponent color computations even for stimuli of moderate contrast. Failure of linearity in these conditions, which are favorable for linear responses of visual system neurons (Derrington & Lennie, 1984), is more surprising.

The present observations differ from some findings in dark-adapted (Larimer et al., 1975; Ejima & Takahashi, 1985) and light-adapted (Cicerone et al., 1975) conditions in that homogeneity is not rejected. Though classification boundaries are not generally planar, the present data suggest that they may be homogeneous in an extended sense: each boundary appears to consist of rays emanating from a neutral point near the origin. In other words, a stimulus that is in equilibrium remains in equilibrium when its difference from the neutral point is scaled. Although this was a consistent feature of classification boundaries, the present data do not provide a decisive test of homogeneity.

Table 1
Repeatability of and model fits to opponent classification boundaries[a]

Condition	Repeat	IDO	Pool/IDO	GWF/IDO
Observer: ES				
Red–green	1.94	1.42	31.9	2.56
Blue–yellow	2.11	1.67	26.2	3.02
White–black	2.17	0.97	16.0	1.61
Observer: KS				
Red–green	2.28	3.05	37.9	4.51
Blue–yellow	4.35	3.09	43.1	3.94
White–black	1.94	1.34	37.1	2.00
Observer: RR				
Red–green	3.01	1.68	31.2	2.95
Blue–yellow	3.77	2.08	29.0	3.02

[a] Each entry indicates the RMS psychometric distance for all data from one observer and one task. Each unit of error indicates a difference between model and measurement equal to the standard deviation of the cumulative Gaussian fit to the classification psychometric function (see Section 2). Repeat refers to the RMS psychometric distance between one equilibrium measurement and one to three repeats of the same measurement. IDO refers to RMS distance between data and predictions of the IDO model fitted independently to data from each background. Pool/IDO refers to RMS distance between data and predictions associated with pooling raw data across backgrounds and fitting the IDO model to pooled data. GWF/IDO refers to RMS distance between data and predictions associated with correcting data for background-dependent neutral points and asymmetric increment/decrement GWF gain, pooling the data, and fitting the IDO model to pooled data (see text for details).

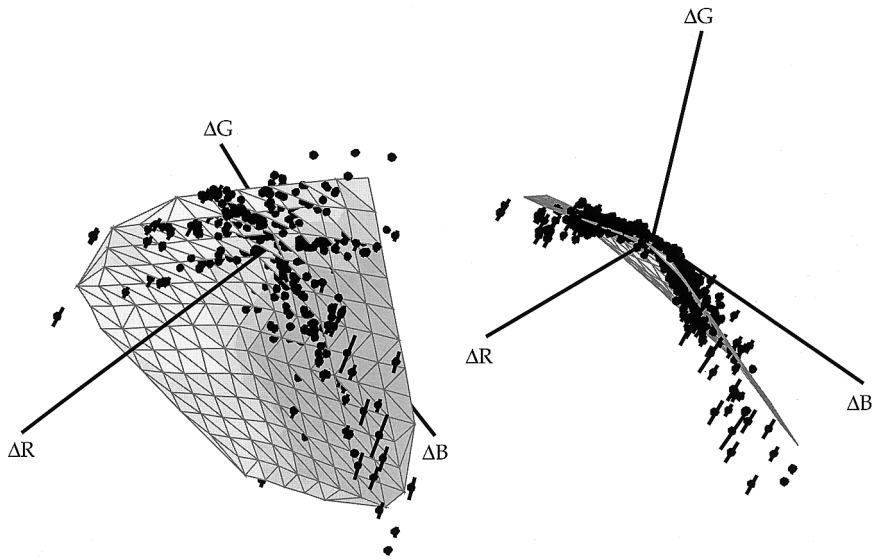

Fig. 10. Pooled and corrected red–green equilibria. The panels show two views of all red–green equilibrium stimuli from one observer expressed in monitor coordinates. 480 equilibrium measurements on 19 different backgrounds are shown. Each datum is expressed as a difference from its respective background, and has been corrected for the best-fitting gain values predicted by the generalized Weber–Fechner model for adaptation. Because of these corrections, axis intensity units are arbitrary. The smooth surface represents the classification boundary predicted by the IDO model. Model parameters were selected to minimize RMS psychometric error. Observer: ES.

4.2. Incomplete discounting of background light

Previous studies have modeled the appearance of a small test stimulus on a large uniform background with two computations: first cone signals at the test location are subject to background-induced sensitivity changes, then the background signal is subtracted at a second stage (possibly color-opponent) (Jameson & Hurvich, 1959; Walraven, 1976; Shevell, 1978). The resulting signal determines appearance. Some authors have suggested that the subtractive process is partial; something similar to the background is subtracted at the second stage (Jameson & Hurvich, 1959; Shevell, 1982). Walraven has defended a more precise and therefore more useful model: the discounting of the background is complete (Walraven, 1976). If this were so, one would expect classification boundaries to include the background, because a transient signal of zero intensity should produce no opponent sensation. The present data sometimes showed deviations from this strong prediction (see Fig. 8), but these deviations were not large enough to determine how the subtracted signal depends on background light.

4.3. Nonlinear models of opponent color signals

The shapes of classification boundaries constrain models of the neural computations that underlie opponent colors. Some classes of nonlinearities may be rejected on purely qualitative considerations. For example, symmetric saturation of increment and decrement cone signals followed by linear opponent combinations cannot explain classification boundary shapes: such a model predicts classification boundaries that are symmetric about the origin, inconsistent with the concave boundary shapes in the present data. Also, the apparent homogeneity in classification boundaries with respect to a neutral point is not predicted by several nonlinear models that have been previously proposed (Larimer et al., 1975; Werner & Wooten, 1979; Elzinga & De Weert, 1984).

DeValois et al. (DeValois & DeValois, 1993; DeValois et al., 1997) recently developed a model of color appearance for simple stimuli which decomposes the red–green and blue–yellow opponent mechanisms into four separate representations corresponding to red, green, blue and yellow. Based on hue scaling data, they argue that S cone signals contribute differently to the red and green mechanisms, and to the blue and yellow mechanisms. Other recent findings have also suggested asymmetries in opposed color signals (Mausfeld & Niederee, 1993; Smith & Pokorny, 1996; Shinomori, Spillmann & Werner, 1998).

A two-stage model based on similar ideas, illustrated schematically in Fig. 12, can be used to describe the shapes of classification boundaries and how they vary with background light. The first part resembles the classical linear model for opponency, except that adaptation separately affects increments and decrements defined with respect to a neutral point. This is motivated by evidence that the gain of increment and decrement visual signals may be controlled independently (Chichilnisky & Wandell, 1996). This asymmetry introduces small bends in the classification boundaries at the

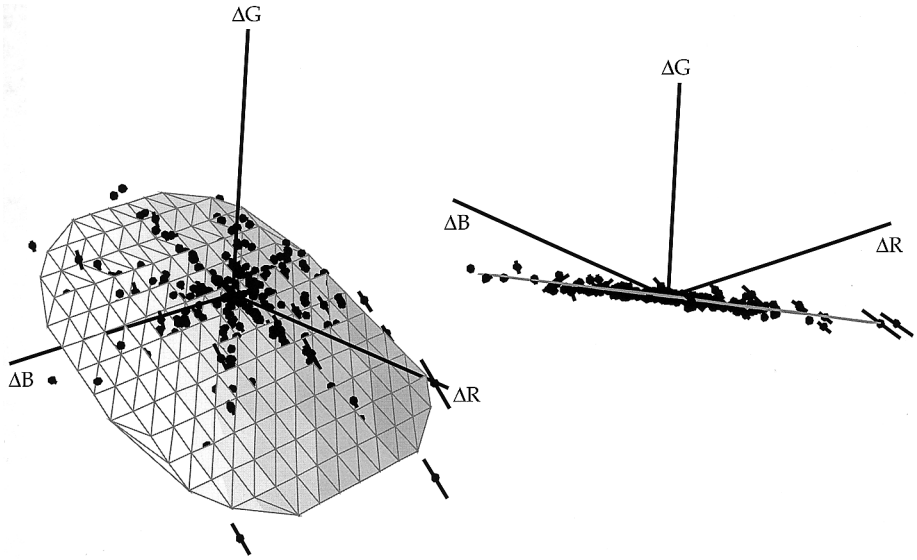

Fig. 11. Pooled and corrected white–black equilibria. A total of 352 equilibrium measurements on 13 different backgrounds are shown. Observer: KS. Other details as in Fig. 10.

transition from increment to decrement cone signals (Mausfeld & Niederee, 1993).

In the second part of the model linear combinations of scaled cone signals are split into increments and decrements to form pre-opponent signals, which are then combined to form opponent signals. This architecture is motivated by the fact that a significant bend in classification boundaries sometimes occurs near the achromatic locus, i.e. the locus of stimuli that appear neither red, green, blue nor yellow (e.g. see Figs. 1 and 2). In the model, crosstalk in the linear combination of pre-opponent signals into opponent signals introduces such a bend in the classification boundary. For example the $BY^{\oplus}$ input to RG shown with dashed lines in the Fig. 12 will give rise to a bend in the red–green boundary at the achromatic locus, because $BY^{\oplus}$ is positive for bluish stimuli and zero for yellowish stimuli.

Because the nonlinearities in this model arise from increment–decrement asymmetries at two stages, the model predicts homogeneous piecewise planar classification boundaries. Separate handling of increment and decrement signals could arise from the half-rectification in visual system neurons.

Since the present results concern equilibrium measurements, which presumably reflect zeroing of opponent signals, they do not constrain models of the magnitude of nonzero opponent signals. For example any model that gives positive values for reddish stimuli and negative values for greenish stimuli suffices to explain red–green equilibria. Judgments of quantities such as saturation, which presumably reflect nonzero opponent signals, would be required to further characterize the opponent computations.

4.4. Physiological color opponency

The present results suggest the need for further investigation of the physiological basis of perceptual color opponency. Prevailing linear models for color opponency motivated the search for *null planes* in parvocellular neurons in the lateral geniculate nucleus (LGN) of macaque monkeys, that is, planes of stimuli in color space that elicit no neural response (Derrington,

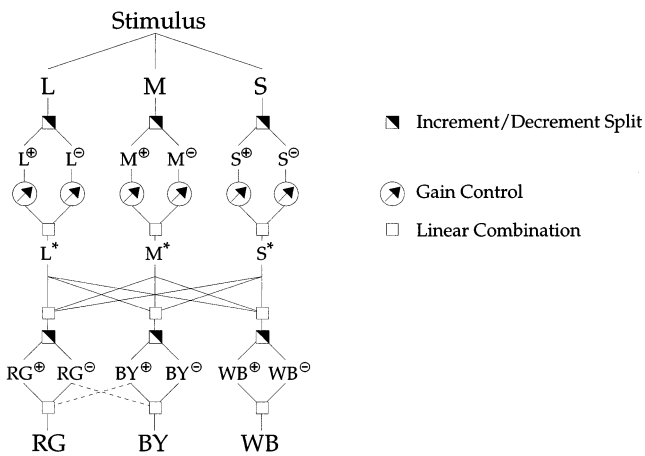

Fig. 12. Model for opponent color classification. Phototransduction in each of the three cone types linearly combines energy at different wavelengths. Linear cone signals ($L\ M\ S$) are split into increment and decrement portions (e.g. $L^{\oplus}$, $L^{\ominus}$) with respect to a neutral point (not shown). The increment and decrement signals are separately scaled by gain factors that depend only on the background light. The intermediate cone signals ($L^*\ M^*\ S^*$) are combined linearly, then separated into increments and decrements to form pairs of pre-opponent signals, e.g. $RG^{\oplus}$, $RG^{\ominus}$. Finally, the pre-opponent signals are combined linearly, with some crosstalk, to create opponent signals, e.g. RG. The signs of the opponent signals control opponent color classification.

Krauskopf & Lennie, 1984). The non-planarity of opponent color classification boundaries raises the possibility that either individual parvocellular LGN neurons are not the neural substrate of perceptual opponency, or that significant nonlinearities in neural responses were overlooked. The present results suggest that a neuron responsible for red–green perception would give no response to a collection of stimuli located on a piecewise planar, but not generally planar, surface in color space. Such *null surfaces* may provide a more exacting test of the role of individual neurons in opponent color perception.

4.5. Limitations

The present conclusions apply to the range of stimulus intensity and saturation available on CRT displays. Because of the relatively low luminance it is possible that weak rod signals played a role in color appearance judgements (Buck, 1997; Stabell & Stabell, 1998). Conclusions about opponent color computations are also limited to conditions of small test stimuli viewed on large uniform backgrounds and may not extend to general images.

The present findings would be affected in some ways if observers had non-standard cone spectral sensitivities not revealed by viewing the Ishihara plates (Ishihara, 1977). Because all stimuli were generated with the three primaries of the CRT, if an observer's cone spectral sensitivities differed from the estimates used here (Stockman et al., 1993), estimates of the cone absorptions associated with stimuli would differ from the actual absorptions by a linear transformation. This error would not affect qualitative conclusions about the shape of classification boundaries. It would affect model fits, which are based on differential scaling of increment and decrement cone signals. Analysis using the Smith and Pokorny cone fundamentals (Smith & Pokorny, 1975) provided nearly identical results.

5. Conclusions

The boundaries separating opponent colors were measured under a variety of adapting conditions, using stimuli of moderate contrast. Classification boundary shapes were generally non-planar, but were summarized with a piecewise planar model. This model suggests hypotheses about the neural mechanisms underlying opponent color computations. The effect of background light on classification boundary shape was largely explained by separate changes in the gain of increment and decrement cone signals.

Acknowledgements

We thank Geoff Boynton and David Brainard for comments on the manuscript. This work was supported by NEI grant R01-EY03164-16 and by the McKnight Foundation. E.J. Chichilnisky was supported by a predoctoral fellowship from the Howard Hughes Medical Institute.

References

Ayama, M., & Ikeda, M. (1986). Additivity of yellow chromatic valence. *Vision Research*, *26*(5), 763–769.

Ayama, M., Kaiser, P., & Nakatsue, T. (1985). Additivity of red chromatic valence. *Vision Research*, *25*(12), 1885–1891.

Brainard, D. H. (1989). Understanding the illuminant's effect on color appearance. PhD dissertation, Stanford University.

Buck, S. L. (1997). Influence of rod signals on hue perception: evidence from successive scotopic contrast. *Vision Research*, *37*(10), 1295–1301.

Burns, S., Elsner, A. E., Pokorny, J., & Smith, V. C. (1984). The Abney effect: chromaticity coordinates of unique and other constant hues. *Vision Research*, *24*, 479–489.

Chichilnisky, E.J. (1995). Perceptual measurements of neural computations in color appearance. PhD dissertation, Stanford University.

Chichilnisky, E. J., & Wandell, B. (1996). Seeing gray through the on and off pathways. *Visual Neuroscience*, *13*, 591–596.

Cicerone, C., Krantz, D., & Larimer, J. (1975). Opponent-process additivity-III. effect of moderate chromatic adaptation. *Vision Research*, *15*, 1125–1135.

DeValois, R. L., & DeValois, K. K. (1993). A multi-stage color model. *Vision Research*, *33*(8), 1053–1065.

DeValois, R. L., DeValois, K. K., Switkes, E., & Mahon, L. (1997). Hue scaling of isoluminant and cone-specific lights. *Vision Research*, *37*(7), 885–897.

Derrington, A., Krauskopf, J., & Lennie, P. (1984). Chromatic mechanisms in lateral geniculate nucleus of macaque. *Journal of Physiology* (*London*), *357*, 241–265.

Derrington, A. M., & Lennie, P. (1984). Spatial and temporal contrast sensitivities of neurones in lateral geniculate nucleus of macaque. *Journal of Physiology* (*London*), *357*, 219–240.

Ejima, Y., & Takahashi, S. (1985). Interaction between short- and longer-wavelength cones in hue cancellation codes: nonlinearities of hue and cancellation as a function of stimulus intensity. *Vision Research*, *25*, 1911–1922.

Elzinga, C., & de Weert, C. M. M. (1984). Nonlinear codes for the yellow/blue mechanism. *Vision Research*, *24*, 911–922.

Fechner, G. (1860). *Elemente der Psychophysik*. Breilkopf and Harterl, Leipzig.

Hering, E. (1878). *Zur Lehre von Lichtsinne*. Carl Gerold's Sohn, Vienna.

Ikeda, M., & Ayama, M. (1980). Additivity of opponent chromatic valence. *Vision Research*, *20*, 995–999.

Ishihara, S. (1977). *Tests for colour-blindness*. Kanehara Shuppen Co. Ltd., Tokyo, Japan.

Jameson, D., & Hurvich, L. M. (1959). Perceived color and its dependence on focal, surrounding, and preceding stimulus variables. *Journal of the Optical Society of America*, *49*, 890–898.

Jameson, D., & Hurvich, L. M. (1955). Some quantitative aspects of an opponent-colors theory. I. chromatic responses and spectral saturation. *Journal of the Optical Society of America*, *45*, 546–552.

Knoblauch, K., Sirovich, L., & Wooten, B. R. (1985). Linearity of hue cancellation in sex-linked dichromacy. *Journal of the Optical Society of America* [*A*], *2*(2), 136–146.

Larimer, J., Krantz, D., & Cicerone, C. (1974). Opponent-process additivity-I. red/green equilibria. *Vision Research*, *14*, 1127–1140.

Larimer, J., Krantz, D., & Cicerone, C. (1975). Opponent process additivity-II. yellow/blue equilibria and non-linear models. *Vision Research*, *15*, 723–731.

Mausfeld, R., & Niederee, R. (1993). An inquiry into relational concepts of colour, based on incremental principles of colour coding for minimal relational stimuli. *Perception*, *22*(4), 427–462.

Shevell, S. K. (1982). Color perception under chromatic adaptation: equilibrium yellow and long-wavelength adaptation. *Vision Research*, *22*, 279–292.

Shevell, S. K. (1978). The dual role of chromatic backgrounds in color perception. *Vision Research*, *18*, 1649–1661.

Shevell, S. K. (1980). Unambiguous evidence for the additive effect in chromatic adaptation. *Vision Research*, *20*, 637–639.

Shinomori, K., Spillmann, L., & Werner, J. (1998). S-cone signals to temporal off-channels: possible asymmetrical connections to postreceptoral chromatic mechanisms. *Vision Research*, *39*(1), 39–49.

Smith, V. C., & Pokorny, J. (1975). Spectral sensitivity of the foveal cone photopigments between 400 and 500 nm. *Vision Research*, *15*, 161–171.

Smith, V. C., & Pokorny, J. (1996). Color contrast under controlled chromatic adaptation reveals opponent rectification. *Vision Research*, *36*(19), 3087–3105.

Stabell, B., & Stabell, U. (1998). Chromatic rod-cone interaction during dark adaptation. *Journal of the Optical Society of America A*, *15*(11), 2809–2815.

Stockman, A., MacLeod, D. I. A., & Johnson, N. E. (1993). Spectral sensitivities of the human cones. *Journal of the Optical Society of America A*, *10*(12), 2491–2521.

Walraven, J. (1976). Discounting the background-the missing link in the explanation of chromatic induction. *Vision Research*, *16*, 289–295.

Walraven, J., & Werner, J. S. (1991). The invariance of unique white; a possible implication for normalizing cone action spectra. *Vision Research*, *31*(12), 2185–2193.

Wandell, B. (1995). *Foundations of vision*. Sinauer, Sunderland, MA.

Watson, A. (1979). Probability summation over time. *Vision Research*, *19*, 515–522.

Werner, J. S., & Walraven, J. (1982). Effect of chromatic adaptation on the achromatic locus: the role of contrast, luminance and background color. *Vision Research*, *22*(8), 929–943.

Werner, J. S., & Wooten, B. R. (1979). Opponent chromatic mechanisms: relation to photopigments and hue naming. *Journal of the Optical Society of America*, *69*(3), 422–434.